Temporal Information of Linear and Nonlinear Lamb Waves for Fatigue Damage Localization: Analysis and Synthesis

Ming Hong, Zhongqing Su, Ye Lu, Li Cheng

HAL Id: hal-01020435
https://hal.inria.fr/hal-01020435

Submitted on 8 Jul 2014

Temporal Information of Linear and Nonlinear Lamb Waves for Fatigue Damage Localization: Analysis and Synthesis

Ming Hong[1,2], Zhongqing Su[*1,3], Ye Lu[2], Li Cheng[1,3]

[1] *Department of Mechanical Engineering, The Hong Kong Polytechnic University, Hong Kong SAR*
[2] *Department of Civil Engineering, Monash University, Clayton, VIC 3800, Australia*
[3] *The Hong Kong Polytechnic University Shenzhen Research Institute, Shenzhen 518057, China*

*mmsu@polyu.edu.hk

ABSTRACT

The time of flight (TOF) features of Lamb waves have been widely applied to locate gross damage in plate structures, which may greatly facilitate the localization process when a sparse sensor network is adopted. Through a time-frequency analysis, this study extends the usage of TOF to nonlinear Lamb waves, taking advantage of their higher sensitivity to small-scale fatigue damage. The precision and practicality of using temporal signal features of linear and nonlinear Lamb waves for fatigue damage characterization are compared. Case studies are conducted on aluminum plates through numerical simulation and experiments, where miniature piezoelectric wafers are networked into a sparse array for Lamb wave excitation and acquisition. A probability-based imaging algorithm is then proposed to visualize damage. Finally, the comparison has motivated a synthesized scheme for locating fatigue damage in various conditions, enhancing the adaptivity of structural health monitoring for real-world applications.

KEYWORDS : *nonlinear Lamb waves, fatigue damage, time of flight, sparse sensor network, structural health monitoring.*

INTRODUCTION

Lamb waves have been employed as a prevailing tool for the structural health monitoring (SHM) of plate-like engineering structures. Of the many techniques developed, the majority relies on waveform changes in the time domain, typified by delays in the time of flight (TOF), wave reflections or transmissions, mode conversions, *etc*. These features usually result from damage-induced alterations of linear material parameters, and thus are referred to as the linear features (of linear Lamb waves). Among these features, the TOF has been widely exploited for accurate localization of gross damage [1,2] with only a few sensors required, while other techniques may need denser networks to achieve the same accuracy. A reasonably optimized sparse sensor network, compared to a dense network, can substantially reduce power consumption and leave minimal impacts on host structures [2].

Meanwhile, continuous efforts have been casted to explore nonlinear Lamb waves for characterizing material degradation and structural damage, particularly small-scale damage, because inherent nonlinearities of the medium/damage, or external modulations, can distort the probing waves and result in nonlinear signals, exhibited through higher- and sub- harmonic generation [3-5], mixed frequency response [6], *etc*. Among these methods, second harmonic generation has been a popular tool for the characterization of fatigue damage [3,7–9] in its early stages, in an effort to prevent structural failure that may follow shortly. As fatigue introduces considerable local nonlinearities in the material, the magnitude of second harmonics may serve as a sensitive indicator to such damage.

In practice, both linear and nonlinear Lamb waves have found respective applications in damage detection, albeit their effectiveness and practicality may be arguable. For example, many linear techniques are not sensitive enough to small-scale damage due to their large probing wavelengths relative to damage sizes [9]; while nonlinear techniques are not subject to the wavelength limit, some of them are essentially impractical, either because bulky wedge transducers have to be used, or a

dense sensor allocation is required for accurate damage localization [8]. Additionally, nonlinear Lamb wave may also be prone to environmental noise. In this study, fatigue damage localization techniques based on temporal information of signals acquired via a sparse sensor network are developed for both linear and nonlinear Lamb waves. Two genres of probability-based damage indices are constructed to locate fatigue cracks in aluminum plates through numerical simulation and experiments, and their precision and practicality are compared. A synthesized scheme is then proposed to combine the two approaches for damage characterization in various conditions. Miniature lead zirconate titanate (PZT) elements are used as a critical step towards embeddable SHM.

1 TOF OF LINEAR LAMB WAVES

1.1 Theory of TOF

The time of flight is the duration for a specific wave packet to travel a certain distance. Often used with a sparse sensor network, TOF-based damage detection processes directly on time-domain signals for localization of damage that are close in size to the probing wavelength.

For illustration, a sensing path $T_i - T_j$ ($i, j = 1, 2, …, N, i \neq j$) from a network composed by N PZT transducers is schematically shown in Figure 1(a). An arbitrary coordinate system is established such that the actuator T_i, the sensor T_j, and the damage are situated at (x_i, y_i), (x_j, y_j), and (x_d, y_d), respectively. Hence, a geometric relationship can be established as

$$\sqrt{(x_d - x_i)^2 + (y_d - y_i)^2}\Big/V_i + \sqrt{(x_d - x_j)^2 + (y_d - y_j)^2}\Big/V_{d-s} - \sqrt{(x_j - x_i)^2 + (y_j - y_i)^2}\Big/V_i = \Delta t_{i-j}, \quad (1)$$

where V_i and V_{d-s} are the group velocities of the incident wave and the damage-scattered wave, respectively, which may or may not be equal (depending on whether mode conversion occurs); and Δt_{i-j} is the difference between i) the TOF for the incident wave to travel from T_i to T_j via the damage, and ii) the TOF for the incident wave to travel directly from T_i to T_j. Therefore, Equation (1) mathematically depicts an elliptical or ellipse-like locus, presenting possible damage locations perceived by path $T_i - T_j$. If multiple sensing paths are available, as in a sensor network, damage locations can be decided at the intersections of the loci from all these paths.

1.2 TOF-based linear DI

In order to combine the damage information obtained from individual sensing paths for thorough assessment, a damage index (DI) is established based on the probability of damage occurrence, covering the entire area under inspection using methods of interpolation and extrapolation [2].

First, the inspected area is virtually meshed with $P \times Q$ nodes (assuming the region is rectangular). To quantify the probability of damage at every spatial node in relation to the locus obtained from individual sensing paths, a cumulative distribution function $F(z)$ is introduced as [1]

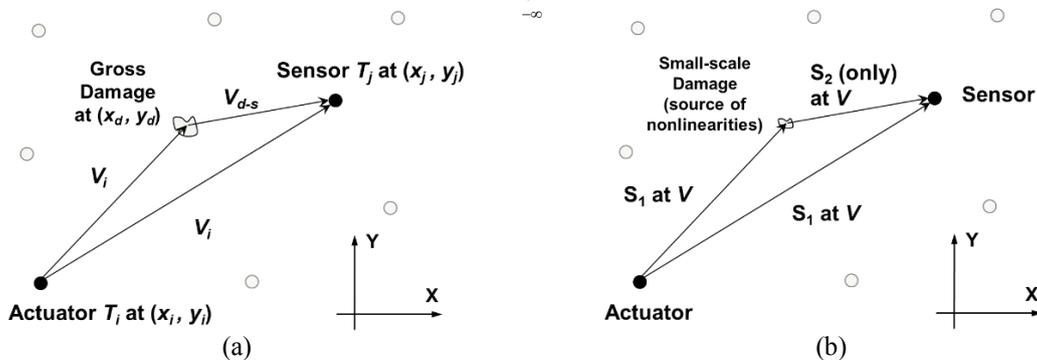$$F(z) = \int_{-\infty}^{z} f(z) \cdot dz, \quad (2)$$

Figure 1: (a) Part of a transducer network with gross damage: the idea of using TOF for damage localization; and (b) using TOF of nonlinear Lamb waves for small-scale damage localization

where

$$f(z_{mn}) = \exp[-z_{mn}^2 / (2\sigma_{mn}^2)] / (\sigma_{mn}\sqrt{2\pi}) \tag{3}$$

is the Gaussian distribution function that represents the probability density of damage occurrence at nodal point (x_m, y_n) $(m = 1, 2, …, P; n = 1, 2, …, Q)$, z_{mn} is the shortest distance from the node to the locus, and σ_{mn} is the standard deviation as a tolerance factor in the imaging process. Equation (2) implies that the closer one node is to the locus of a particular path, the higher the probability is at that node. Thus, the field value of DI at point (x_m, y_n) perceived by path $T_i - T_j$ is determined as

$$DI_{i,j}(x_m, y_n) = 1 - [F(z_{mn}) - F(-z_{mn})]. \tag{4}$$

Finally, combining information from all the sensing paths in the network, the ultimate diagnostic image, using linear Lamb waves, is produced through an image fusion scheme [10] of the DIs, as

$$DI_{Linear} = \frac{1}{N(N-1)} \sum_{i,j=1, i \neq j}^{N} DI_{i,j}. \tag{5}$$

After visualization, pixels with remarkably high values would highlight the damage zone, providing quantitative depiction about its location, size and even orientation. As mentioned earlier, this localization algorithm is most effective when the damage is gross enough to induce damage scattering that can be distinguished directly in the time domain.

2 TOF OF NONLINEAR LAMB WAVES

To take advantage of its high sensitivity to small-scale damage, a novel DI based on the TOF of nonlinear Lamb wave features is established in this study for fatigue damage localization, adopting the same philosophy of sparse PZT sensor networks from the linear technique above.

2.1 Nonlinear Lamb waves

An elastic plate may contain certain types of nonlinearities that distort guided Lamb waves, producing higher-order harmonics (*e.g.*, second harmonics). Specifically, the intact material itself possesses a weak mesoscopic nonlinearity over the entire domain [11]. As fatigue emerges, microstructure defects such as dislocations accumulate under cyclic loading, forming persistent slip bands that may nucleate micro-cracks. Throughout this process, localized, yet more pronounced nonlinearities are introduced in the damage's vicinity, leading to strengthened nonlinear wave effects. Detailed studies can be found [12,13] on the types of nonlinearities and their mechanisms. Here, it is assumed that all of these nonlinearities are localized indications of fatigue, which contribute collectively to the strengthening of second harmonics of Lamb waves passing through the damaged region.

The acoustic nonlinearity parameter, β, is usually adopted to calibrate the nonlinearity of Lamb waves. This parameter is theoretically derived from the nonlinear stress-strain relation of a material containing nonlinearities (*e.g.*, damage). Meanwhile, it also links the amplitudes of the probing fundamental mode (A_1) and its paired second harmonic mode (A_2), according to

$$A_2 = 1/8 A_1^2 k^2 x \cdot \gamma \cdot \beta, \tag{6}$$

where k and x are the wavenumber and particle location, respectively; γ is a Lamb wave scaling function that does not vary with respect to the health state of the medium [4]. Equation (6) shows that stronger nonlinear effects around fatigue damage (manifested by an increase in β) would enlarge the amplitude of the second harmonics, assuming the fundamental mode is barely impacted.

Note that, due to the multimodal and dispersive natures of Lamb waves, only one selected wave mode at each interested frequency would be exploited. In order to achieve strong and cumulative harmonic generation upon nonlinear distortion, the probing fundamental mode at the excitation frequency f and its paired second harmonic mode at $2f$ should share (roughly) the same phase and group velocities, a condition termed synchronism, with non-zero power flux in between. In this study, (S_1, S_2) in aluminum 6061-T6, a popular choice, is considered, of which the S_1 mode is excited at a

frequency-thickness product of 3.59 MHz·mm and travels at 4,375 m/s, and S_2, at 7.18 MHz·mm, is the corresponding second harmonics of S_1 with the same velocity. One advantage of using (S_1, S_2) is that both modes are the fastest at their corresponding frequencies and hence can be easily spotted.

2.2   TOF-based nonlinear DI

To construct a DI using the TOF of nonlinear Lamb wave features, a selective mode is first excited at a central frequency of f in the inspected plate in both benchmark and current conditions, according to the requirement of synchronism. Subsequently, a time-frequency analysis is performed to extract two amplitude (energy) profiles from each signal as two functions of time at f and $2f$, respectively, for comparison. At $2f$, on one hand, an indicative event, such as an abrupt energy hump, can be found at some point in the current signal, presenting deviations from the benchmark. Such an energy packet is generated when the incident wave is nonlinearly distorted by the damage, which acts as a new source emitting added second harmonics to the sensor. On the other hand, at f, the two amplitudes would barely deviate from each other (so will not the original time histories), until the damage size has approached the wavelength of the fundamental mode to induce significant damage scattering. Figure 1(b) illustrates this idea using mode pair (S_1, S_2). Now, Equation (1) can be directly applied to the nonlinear case, with $V_i = V_{d-s} = V_{S_1} = V_{S_2}$. The subsequent steps would be identical to the linear method, leading to a final damage index $DI_{Nonlinear}$, which utilizes the TOF of the second harmonic features for damage diagnosis. Detailed signal processing can be found in Section 3.3.

Note that the amount of energy shift is considered trivial, relative to the dominant wave energy at the fundamental frequency; it is nonetheless clearly evidenced at the double frequency, which is weaker in the first place, facilitating the recognition of TOF features through second harmonics.

3   SIMULATION CASE STUDY

In this section, the linear and nonlinear DIs are applied comparatively on data from finite element (FE) simulation, to evaluate a 1-mm fatigue crack in an aluminum plate with local nonlinearities.

The aluminum plate under investigation ($450 \times 300 \times 3.18$ mm^3, 6061-T6), as schematically shown in Figure 2(a), is created and analyzed using Abaqus. A 10-mm rivet hole is produced to serve as the fatigue crack initiator, centered at (25 mm, 45 mm). Four circular PZT wafers, 8 mm in diameter, are collocated on one side of the plate to form six sensing paths. For the damaged condition, a 1-mm long, through-thickness crack is created, running down from the bottom of the hole in Y direction with an initial surface clearance of zero. The in-plane midpoint of the crack is at (25 mm, 39.5 mm).

Next, C3D8R elements, each sized at 0.2 mm in plane, are used to mesh the plate, as displayed in Figure 2(b). PZT wafers are modeled by disk-like objects tied to the plate surface. 15.5-cycle Hann-windowed sinusoidal tone bursts at $f = 1,130$ kHz are excited by imposing uniform in-plane radial displacements on the actuator's periphery; this particular frequency actuates S_1 as the probing fundamental mode, given the plate thickness of 3.18 mm. Responses are acquired by the sensors in the form of in-plane strains, and excitation is performed on each wafer in turn. Assuming wave
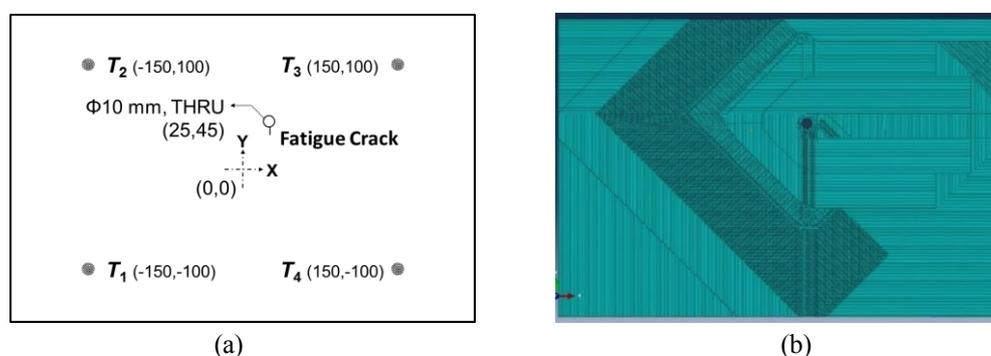

(a)   (b)

Figure 2: (a) Schematic of the simulated aluminum plate with a rivet hole and four transducers (in *mm*, crack length exaggerated); and (b) meshed FE model of the plate.

reversibility (given the same velocity of S_1 and S_2), only one signal is required from each of the paths.

For the damaged case, mesoscopic and plastic nonlinearities are introduced by modifying the material constitutive equation [13]. A seam definition, with contact properties, is imposed on the physical crack to induce the "breathing" behavior and other local nonlinear effects.

3.1 Linear DI result

For linear Lamb waves, although the excitation frequency needs not to be exactly 1,130 kHz, this frequency does give good signal recognizability with well separated wave packets. Figure 3(a) displays typical time histories via path $T_1 - T_4$ before and after the inclusion of damage, which shows no apparent damage-scattered waves in the current signal, because even at such a high frequency, the probing wavelength of S_1 (~3.9 mm) is still not precise enough to characterize a 1-mm crack. Consequently, the TOF values retrieved from the time histories contain considerable uncertainties, and σ_{mn} in Eq. (3) is thus set at a large value to account for the lack of confidence in the results. As shown in Figure 3(b), the calculated DI_{Linear} renders false predictions in the final diagnostic image.

3.2 Nonlinear DI result

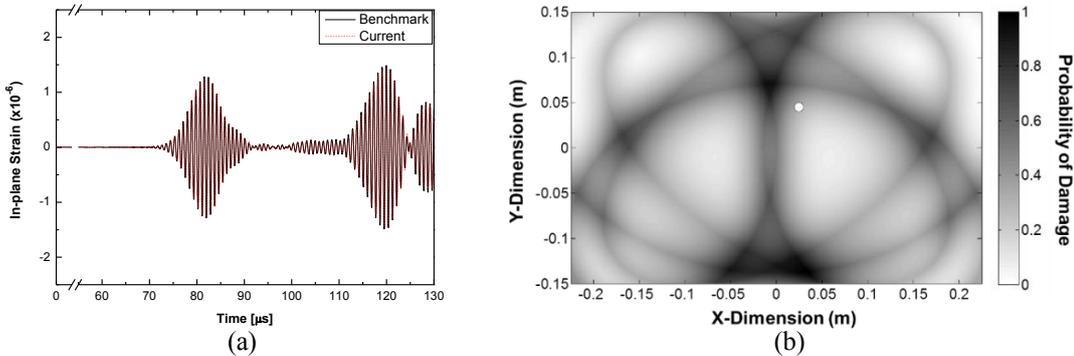While difficulties exist in finding damage-scattered waves in time histories, as shown by Figure 3(a),

(a)   (b)

Figure 3: (a) Time series via $T_1 - T_4$; and (b) Imaging using TOFs of linear signals from simulation.

(a)   (b)

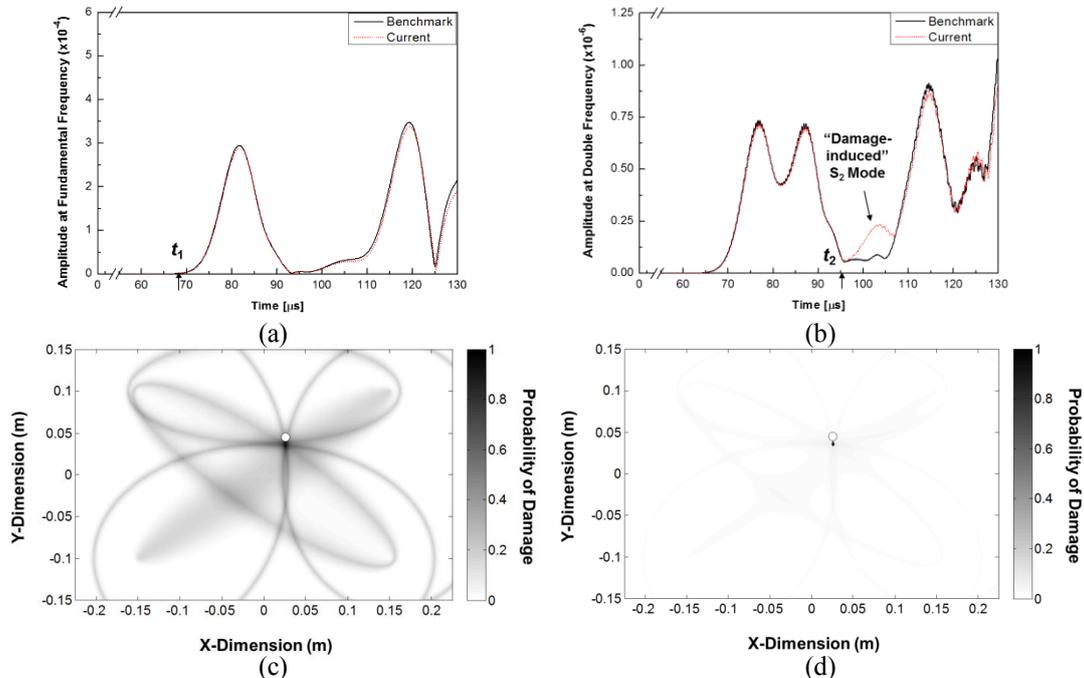(c)   (d)

Figure 4: Amplitude profiles of signals via $T_1 - T_4$ at (a) fundamental frequency, and (b) double frequency; (c) a raw diagnostic image using TOFs of second harmonic features; and (d) improved imaging with $\kappa = 0.9$

the short-time Fourier transform (STFT) is performed on the two signals to generate spectrograms that contain both time and frequency information. Next, two slices are cut from each of the spectrograms at f and $2f$, respectively, and then plotted as functions of time in Figures 4(a) and 4(b). The almost overlapping amplitude profiles at f confirms that no significant damage-scattering has occurred in the time series. At $2f$, it is noticed that second harmonics are already presented in the benchmark signal, part of which comes from the weak mesoscopic nonlinearity of the intact medium, with the rest presumably generated by the mathematical nonlinearities involved in the FE program which are irrelevant to the cumulative generation (*i.e.*, $S_1 \rightarrow S_2$) described earlier. However, Figure 4(b) clearly reveals a strengthened hump in the current signal. This second harmonic packet is considered the S_2 mode generated from the probing S_1 mode upon its interaction with the damage.

Thus, using the TOF of S_2 at $2f$ (t_2 in Figure 4(b)) and the TOF of S_1 at f (t_1 in Figure 4(a)), and following Equations (1) through (4), $DI_{Nonlinear}$ can be determined for this sensing path. Finally, by fusing individual DIs from each path in the network, a raw diagnostic image is produced in Figure 4(c). In addition to the adjustment of σ_{mn}, a threshold κ can be applied to reinforce the identification result, which is a preset percentage of the maximum field value of the final image such that any field value less than the threshold is forced to approach zero. Figure 4(d) shows the final image with $\kappa = 90\%$, in which the location and rough size of the fatigue crack is successfully highlighted. This result verifies the feasibility of the proposed localization algorithm using the TOF of nonlinear Lamb waves.

4   EXPERIMENTAL CASE STUDY

Following the simulation, the TOF of linear and nonlinear Lamb waves are reinvestigated to experimentally evaluate a 3-mm fatigue crack in an aluminum plate.

Four PZT wafers (8 mm in diameter each) are first surface-mounted on an intact 6061-T6 aluminum plate as photographed in Figure 5(a), which is consistent with the schematic of Figure 2(a). The same excitation signal from the simulation is applied on the actuator, by a Tektronix 3000C arbitrary function generator. No power amplifiers are used in the experiment in order to reduce possible harmonic distortion during amplification. The response signals are acquired by the other three wafers through a Tektronix 4034B oscilloscope at a sampling rate of 100 MS/s with 512-time averaging. As with the simulation, excitation is repeated on each wafer for the benchmark condition.

To produce fatigue damage, the specimen has first undergone a high-cycle fatigue testing on an Instron 8802 fatigue platform, subject to a sinusoidal tensile load varying from 2 to 20 kN at 10 Hz. To facilitate the initiation of cracks, a tiny, yet sharp notch is inscribed at the bottom edge of the rivet hole. After roughly 1.2-million cycles, a barely visible fatigue crack in parallel with the 300-mm side is produced, measuring about 3 mm in length through the thickness, as shown in Figure 5(b). The same signal excitation and acquisition procedure is performed on the damaged specimen.

4.1   Linear *versus* nonlinear DIs

After necessary preprocessing such as low-pass filtering, all the experimental signals are processed through STFT. In Figures 6(a) and 6(b), the amplitudes profiles of two typical signals (benchmark and current, via path $T_1 - T_4$) are respectively displayed. As can be seen, the profiles at the fundamental frequency exhibit deviations after the first S_1 packet, because the crack size is close

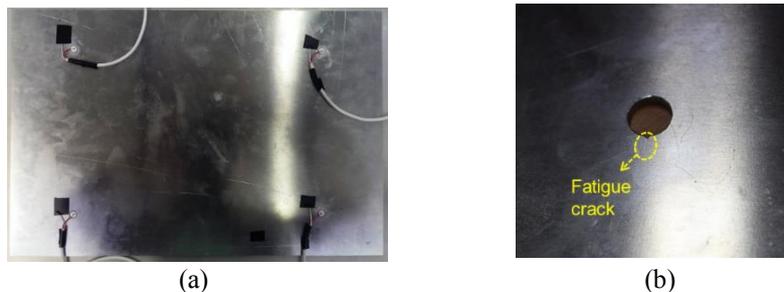| (a) | (b) |

Figure 5: (a) Aluminum plate with a rivet hole; and (b) barely visible crack after fatigue testing

enough to the probing wavelength to incur damage scattering. By finding the TOF of damage-scattered waves (from either the time histories or the amplitude profiles), DI_{Linear} can be determined for each sensing path and then fused to construct the final diagnostic image, as shown in Figure 6(c). Compared to the simulation case where the crack is only 1-mm long, the localization for this bigger crack is significantly improved using linear Lamb waves.

As shown in Figure 6(b), though, deviations of amplitude profiles at the double frequency are more distinguishable, with enhanced second harmonics standing out at a particular time point. This observation confirms the higher sensitivity of second harmonics to fatigue damage, and provides useful TOF information for damage localization. Likewise, the $DI_{Nonlinear}$ is developed based on the TOF of the second harmonics and a final diagnostic image is presented in Figure 6(d). The linear and nonlinear results have shown good agreement in this case.

4.2 Synthesis of DIs

In the above, the TOF technique is used to process both linear and nonlinear Lamb waves acquired from a sparse sensor network. For smaller damage, the nonlinear DI outperforms its linear counterpart with a higher damage sensitivity. However, this sensitivity roots in the fact that the energy level of the double frequency is significantly lower than that of the fundamental frequency in the first place. If noise in the signal gets to a considerable magnitude, as they would in practice, useful second harmonic features might be inundated, leaving the nonlinear DI less credible. In this regard, the linear technique is more noise-tolerant. For this reason, a synthesized damage localization and SHM
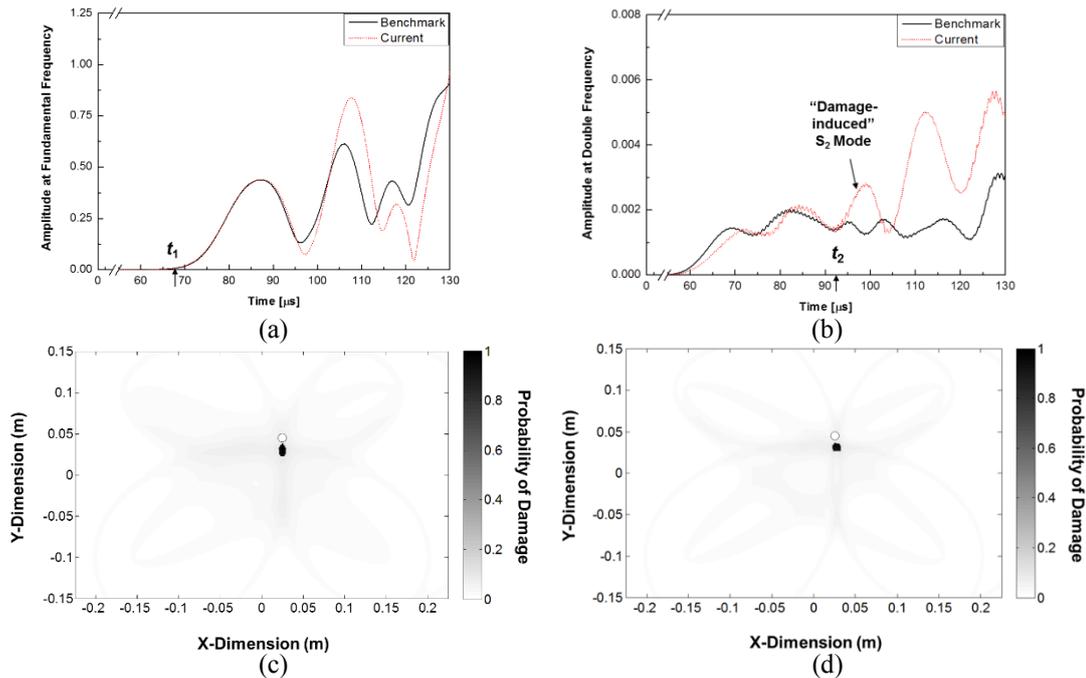

Figure 6: Amplitude profiles of experimental signals via $T_1 - T_4$ at (a) fundamental frequency, and (b) double frequency; and diagnostic images using TOFs of (c) linear signals, and (d) nonlinear signals, both with $\kappa = 0.9$
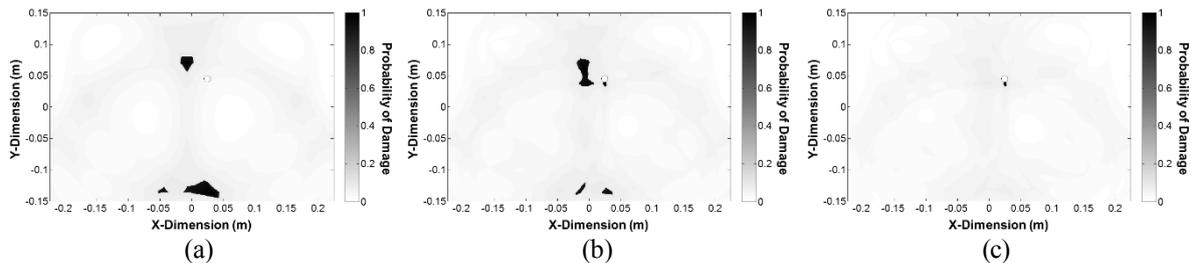

Figure 7: Diagnostic images using DI_S with (a) $w_{NL} = 0$; (b) $w_{NL} = 0.4$; and (c) $w_{NL} = 0.5$ ($\kappa = 0.9$ for all)

strategy is proposed to deal with various crack sizes and ambient environments.

The synthesized damage index DI_S is obtained as a weighted average of DI_{Linear} and $DI_{Nonlinear}$:

$$DI_S = w_L \cdot DI_{Linear} + w_{NL} \cdot DI_{Nonlinear} , \qquad (7)$$

where w_L and w_{NL} are the weights for the linear and nonlinear DIs, respectively, which sum to 1. The weights are assigned based on the stage of damage and/or the noise level. Figure 7 illustrates three diagnostic examples from the simulation (where the crack is small and noise is not influential), with $w_{NZ} = 0$, 0.4, and 0.5, respectively. As can be seen, when the crack is too small to be depicted solely by DI_{Linear}, small adjustments of the weights can make immediate improvement to the final image using DI_S. At $w_{NZ} = 0.5$, the fatigue damage has been successfully located and clearly indicated.

CONCLUSIONS

The TOF features of linear and nonlinear Lamb waves are investigated for fatigue damage localization in aluminum plates, using a sparse sensor network. Two genres of damage indices are established through a probabilistic imaging algorithm. Case studies are conducted via simulation and experiment on fatigued aluminum plates. While the linear TOF technique is straightforward and effective with gross damage, it fails to identify small-scale damage whose size is much smaller than the probing wavelength. A synthesized DI is finally proposed to combine nonlinear Lamb waves' high sensitivity to small-scale damage with the high noise-tolerance of the linear technique, enabling the approach for adaptive SHM, where potential influences of crack growth and ambient noise are of concern.

ACKNOWLEDGMENTS

REFERENCES

[1] Z. Su, L. Cheng, X. Wang, L. Yu, C. Zhou. Predicting delamination of composite laminates using an imaging approach. *Smart Mater. Struct.*, 18: 074002, 2009.

[2] Z. Su, L. Ye. *Identification of damage using Lamb waves*. Springer, 2009.

[3] C. Pruell, J.-Y. Kim, J. Qu, J. L. Jacobs. Evaluation of fatigue damage using nonlinear guided waves. *Smart Mater. Struct.*, 18: 035003, 2009.

[4] Y. Xiang, M. Deng, F.-Z. Xuan, C.-J. Liu. Experimental study of thermal degradation in ferritic Cr-Ni alloy steel plates using nonlinear Lamb waves. *NDT E. Int.*, 44: 768-774, 2011.

[5] I. Solodov, J. Wackerl, K. Pfleiderer, G. Busse. Nonlinear self-modulation and subharmonic acoustic spectroscopy for damage detection and location. *Appl. Phys. Lett.*, 84:5386-5388, 2004.

[6] F. Aymerich, W. J. Staszewski. Experimental study of impact-damage detection in composite laminates using a cross-modulation vibro-acoustic technique. *Struct. Health Monit.*, 9: 541-553, 2010.

[7] K.-Y. Jhang. Nonlinear ultrasonic techniques for non-destructive assessment of micro damage in material: a review. *Int. J. Precis. Eng. Manuf.*, 10: 123-135, 2009.

[8] C. Zhou, M. Hong, Z. Su, Q. Wang, L. Cheng. Evaluation of fatigue cracks using nonlinearities of acousto-ultrasonic waves acquired by an active sensor network. *Smart Mater. Struct.*, 22: 015015, 2013.

[9] Z. Su, C. Zhou, M. Hong, L. Cheng, Q. Wang, X. Qing. Acousto-ultrasonics-based fatigue damage characterization: Linear versus nonlinear signal features. *Mech. Syst. Signal Process.*, 45: 225-239, 2014.

[10] C. Zhou, Z. Su, L. Cheng. Probability-based diagnostic imaging using hybrid features extracted from ultrasonic Lamb wave signals. *Smart Mater. Struct.*, 20: 125005, 2011.

[11] Y. Shen, V. Giurgiutiu. Predictive modeling of nonlinear wave propagation for structural health monitoring with piezoelectric wafer active sensors. *J. Intell. Mater. Syst. Struct.*, 25: 506-520, 2014.

[12] D. Broda, W. J. Staszewski, A. Martowicz, T. Uhl, V. V. Silberschmidt. Modelling of nonlinear crack-wave interactions for damage detection based on ultrasound–a review. *J. Sound Vib.*, 333: 1097-1118, 2014.

[13] M. Hong, Z. Su, Q. Wang, L. Cheng, X. Qing. Modeling nonlinearities of ultrasonic waves for fatigue damage characterization: Theory, simulation, and experimental validation. *Ultrasonics*, 54: 770–778 2013.